11252 *Biochemistry* **2009,** *48,* 11252–11263
DOI: 10.1021/bi901548c

BIOCHEMISTRY
including biophysical chemistry & molecular biology
Article

Critical Role of Tryptophan 154 for the Activity and Stability of Class D β-Lactamases[†,‡]

Stéphane Baurin,[§,△] Lionel Vercheval,[§,△] Fabrice Bouillenne,[∥] Claudia Falzone,[⊥] Alain Brans,[∥] Lilian Jacquamet,[#] Jean-Luc Ferrer,[#] Eric Sauvage,[⊥] Dominique Dehareng,[∥] Jean-Marie Frère,[∥] Paulette Charlier,[⊥] Moreno Galleni,*[,§] and Frédéric Kerff*[,⊥]

[§]*Laboratory of Biological Macromolecules and* [∥]*Laboratory of Enzymology and* [⊥]*Laboratory of Protein Crystallography, Center for Protein Engineering, University of Liège, Institut de Chimie B6a, 4000, Liège, Belgium, and* [#]*Laboratoire de Crystallographie et Crystallogenèse des Protéines, Institut de Biologie Structurale J.-P. Ebel, CEA/CNRS/UJ.F, 38027 Grenoble Cedex 1, France.* [△]*Both authors contributed equally to this work.*

Received September 4, 2009; Revised Manuscript Received October 27, 2009

ABSTRACT: The catalytic efficiency of the class D β-lactamase OXA-10 depends critically on an unusual carboxylated lysine as the general base residue for both the enzyme acylation and deacylation steps of catalysis. Evidence is presented that the interaction between the indole group of Trp154 and the carboxylated lysine is essential for the stability of the posttranslationally modified Lys70. Substitution of Trp154 by Gly, Ala, or Phe yielded noncarboxylated enzymes which displayed poor catalytic efficiencies and reduced stability when compared to the wild-type OXA-10. The W154H mutant was partially carboxylated. In addition, the maximum values of k_{cat} and k_{cat}/K_M were shifted toward pH 7, indicating that the carboxylation state of Lys70 is dependent on the protonation level of the histidine. A comparison of the three-dimensional structures of the different proteins also indicated that the Trp154 mutations did not modify the overall structures of OXA-10 but induced an increased flexibility of the Ω-loop in the active site. Finally, the deacylation-impaired W154A mutant was used to determine the structure of the acyl-enzyme complex with benzylpenicillin. These results indicate a role of the Lys70 carboxylation during the deacylation step and emphasize the importance of Trp154 for the ideal positioning of active site residues leading to an optimum activity.

Bacterial resistance of Gram-negative bacteria toward β-lactam antibiotics is mainly due to the production of β-lactamases, enzymes which efficiently hydrolyze the β-lactam amide bond (*1*). To date, more than 700 different β-lactamases are described. They are classified in two families, the active site serine β-lactamases and the metallo-β-lactamases (*2*). Based on their amino acid sequences, the active site serine β-lactamases are divided into three molecular classes: A (*2*), C (*3*), and D (*4*). Unlike class A and C enzymes which were extensively studied (*5*−*9*), less information is available on class D β-lactamases. They are known as oxacillinases (OXA) since they generally exhibit hydrolytic activity against isoxazolylpenicillins (oxacillin), methicillin, or extended-spectrum cephalosporins and they are poorly inhibited by clavulanic acid (*10*−*12*). Recently, an increasing number of OXA enzymes displaying a carbapenemase activity have been isolated (*13*−*16*). Interestingly, the hydrolysis of a large number of substrates is generally characterized by biphasic kinetics with a burst (*11*).

The majority of class D β-lactamase genes is plasmid encoded and is found in clinically relevant Gram-negative bacteria such as *Pseudomonas aeruginosa* (*17*). In recent years, several oxacillinase genes were found on the chromosome of several environmental species (*18*, *19*). Their production can be either constitutive or induced by the presence of a β-lactam in the culture medium (*19*). The class D β-lactamases are monomeric (like OXA-1) (*20*) or dimeric (OXA-29) (*18*). In the case of OXA-10, an equilibrium between the two forms has been observed (*11*). This equilibrium is influenced by the protein concentration and also external conditions such as pH or the presence of metal ions. The dimer/monomer dissociation constant has been estimated to 1 μM (*21*). The activity of class D β-lactamases is affected by different cofactors such as divalent metal ions (Co^{2+}, Cd^{2+}, Cu^{2+}) (*22*), sodium chloride (NaCl), and sodium bicarbonate ($NaHCO_3$) (*22*, *23*). The addition of divalent metal cations stabilizes the dimeric form and increases the enzyme stability (*22*, *24*). NaCl behaves generally as a competitive inhibitor. Finally, the addition of $NaHCO_3$ can abolish the biphasic kinetics and activate the enzyme (*21*). The structures of the different classes of the active site serine β-lactamases share a similar fold made of two domains: an α domain which contains

[†]The project was supported by the European Commission Sixth Framework Program grant LSMH-CT-COBRA 2003-503335, by the Belgian Program of Interuniversity Poles of Attraction initiated by the Belgian State, Prime Minister's Office, Science Policy programming (IAP no. P6/19), by the Fonds de la Recherche Scientifique (FRS-FNRS) (FRFC no. 2.4.508.01.F, 9.4.538.03.F, 2.4.524.03, 2.4561.07), and by the University of Liège (Fonds spéciaux, Crédit classique, 1999). S.B. and L.V. are Ph.D. students financed by the Fonds de la Recherche pour l'Industrie et l'Agriculture (F.R.I.A). F.K. is Chargé de Recherche of the FRS-FNRS. Use of the FIP/BM30a beamline was supported by the FRS-FNRS under Contract IISN 4.4505.00.

[‡]The coordinates and structure factors have been deposited in the Protein Data Bank, and the PDB accession codes are 2HP5 for the OXA-10 W154G mutant at pH 7.0, 2RL3 for the OXA-10 W154H mutant at pH 7.0, 2WGI for the complex W154A-PenG, and 2HP6, 2HP9, and 2HPB for the OXA-10 W154A mutant at pH 7.5, 6.0, and 9.0, respectively.

*To whom correspondence should be addressed. G.M.: tel, +32 4 366 3549; fax, + 32 4 366 3364; e-mail, mgalleni@ulg.ac.be. K.F.: tel, +32 4 366 3620; fax, + 32 4 366 3748; e-mail, fkerff@ulg.ac.be.

 Published on Web 10/27/2009

only helices and an α/β domain which contains an antiparallel β-sheet and the C- and N-terminal helices (*25*−*28*). The active site lies at the junction between the two domains. Among all known class D enzymes, three conserved motifs are found, Ser67-Xaa-Xaa-Lys70 where Ser67 is the active serine, Ser115-Xaa-Val117, and Lys205-Thr/Ser-Gly207. In addition, Trp154 located on an Ω-loop (residues 147−156) is well conserved. Analysis of the different available three-dimensional structures of OXA-10 shows that Lys70 may be carboxylated due to a reaction between the ε-NH_2 of the lysine and carbon dioxide (*28*) as shown in the scheme:

$$\varepsilon\text{-}NH_2 + CO_2 + H_2O \rightleftharpoons \varepsilon\text{-}NH{-}COO^- + H_3O^+$$

The carboxylation of a lysine residue is pH dependent and is a compromise between its deprotonation, favored by high pH, and the availability of CO_2, favored by low pH.

This posttranslational modification induces some structural modifications of the active site. A carboxylated Lys70 is observed in both monomers of the biological dimer above pH 7.5 (PDB ID: 1K4F, 1K4E (pH 9.0), 1E4D (pH 8.3), 1K55 (pH 7.5)) (*21*, *28*). A mixed situation where Lys70 is either carboxylated or noncarboxylated, depending of the monomer, is observed at pH between 7 and 6 (PDB ID: 1K56 (pH 6.5), 1K57 (pH 6.0)) (*21*). Under pH 6.0, a noncarboxylated Lys70 prevails (*21*). This situation induces a reorganization of the hydrogen bonds between the essential residues in the active site. Indeed, a slight modification of the loop bearing the second conserved motif is observed and, in a lesser way, of the orientation of the Lys70 ε-amine group and the active Ser67 hydroxyl group.

The comparison of carboxylated and noncarboxylated active sites also shows that the carboxyl group of the modified lysine is hydrogen-bonded with the indole group of Trp154. This interaction stabilizes the position of the Lys70 side chain and decreases the flexibility of the Ω-loop which influences the accessibility of the active site. Indeed, in the OXA-1 group, the mutation of Asp66, which makes a stabilizing hydrogen bond with the Ω-loop, induces a decrease of the catalytic activity (*29*). The nonenzymatic carboxylation of a lysine side chain remains a rarely observed phenomenon. A few X-ray structures have revealed carboxylated lysines. In most cases, their roles are essentially structural. In these structures, the carboxylated lysines are stabilized as ligands of active site metal ions, either a Mg^{2+} ion as in MurE (*30*), the ribulose biphosphate carboxylase/oxygenase from spinach Rubisco (*31*), and dihydrofolate synthetase (*32*) or a Co^{2+} ion as in transcarboxylase (*33*) or a Ni^{2+} ion as in urease (*34*). Alanine racemase (*35*), with the class D β-lactamases, is the only example of an enzyme possessing a carboxylated lysine involved in the catalytic activity. In the case of the OXA enzymes, the carboxylated Lys70 acts as a general base during the hydrolysis of the β-lactam and therefore plays an essential catalytic function (*28*).

In this report, we studied the role of Trp154 in the stability and activity of the OXA-10 β-lactamase. OXA-10 is part of the group I of class D β-lactamases and was chosen because it is the most studied of its class and is easy to produce, purify, and crystallize, and clinically relevant strains are expressing variants of OXA-10 with an extended spectrum β-lactamases activity (*24*, *36*). Our results indicate that the replacement of Trp154 by other residues decreases the affinity of OXA-10 toward carbon dioxide. In consequence, OXA-10 mutants were less stable and active despite a conserved tertiary structure. This reduced activity of the W154A mutant allowed us to trap and solve the structure of an acyl-enzyme complex with benzylpenicillin.

MATERIALS AND METHODS

Bacterial Strains, Plasmids, and Media. *Escherichia coli* DH5α and BL21(DE3) Star strains were used for genetic constructions and protein overproduction, respectively. The pGEM-T-easy plasmid was obtained from Promega (Leiden, The Netherlands). The pMON234::pBGS18+ vector which contains the bla_{OXA-10} was a gift of Dr. Levesque (*37*). Cultures were realized in Luria−Bertani (LB)[1] media and in Hopwood minimal media (*38*).

Chemicals. Cloxacillin, oxacillin, cephalothin, and cephaloridine were from Sigma (St. Louis, MO). Benzylpenicillin and nitrocefin were purchased from Rhône-Poulenc (Paris, France) and OXOID (Basingstoke, Hants, U.K.), respectively.

Plasmid Construction. The pMON234::pBGS18+ vector encoding *P. aeruginosa* OXA-10 class D β-lactamase (*37*) was used as template to introduce by PCR the *Nco*I and *Bam*HI restriction sites at the beginning and the end of the gene bla_{OXA-10}, respectively. The PCR was realized in the presence of the primers OXA-10*Nco*I and OXA-10*Bam*HI (Supporting Information Table S1) and a mix of Pfu and Taq polymerases. The amplified fragment which contains bla_{OXA-10} was gel-purified and introduced into the pGEM-T-easy plasmid yielding the pCIPBS1 vector. The gene was sequenced completely to verify the insertion of the *Nco*I and *Bam*HI restrictions sites and the absence of additional mutations. pCIPBS1 was digested by *Nco*I and *Bam*HI restriction enzymes. The 758 bp DNA fragment was gel-purified and ligated into the pET22b Kan^R plasmid digested with the same restriction enzymes, yielding the pET22bla_{OXA-10}.

Site-Directed Mutagenesis. The W154G, W154A, W154F, and W154H mutants of the OXA-10 class D β-lactamase were obtained with the help of the QuikChange site-directed mutagenesis kit. The mutations were performed on pCIPBS1. The mutagenic primers (upstream and downstream) are shown in Supporting Information Table S1. After plasmid amplification and *Dpn*I digestion, *E. coli* DH5α cells were transformed. Colonies were isolated on LB agar plates containing 100 μg/mL ampicillin. The plasmids were isolated, and mutations were identified by DNA sequencing. We selected the plasmids pCIPBS2, pCIPBS3, pCIPBS4, and pCIPLV4 which contained the gene for the W154G, W154A, W154F, and W154H OXA-10, respectively. All plasmids were digested by *Nco*I and *Bam*HI restriction enzymes. The 758 bp DNA fragments were gel-purified and ligated into the pET22b Kan^R plasmid digested with the same restriction enzymes, yielding plasmids pCIPBS6, pCIPBS7, pCIPBS8, and pCIPLV8, producing W154G, W154A, W154F, and W154H OXA-10 mutants, respectively. The different plasmids were introduced into *E. coli* BL21(DE3) Star.

Enzyme Purification. The *E. coli* BL21(DE3) Star carrying the pET22b/bla_{OXA-10}, pCIPBS6, pCIPBS7, pCIPBS8, and pCIPLV8, respectively, were inoculated into 500 mL of LB media. The cultures were incubated overnight at 37 °C in the presence of kanamycin (50 μg/mL) and then added to 15 L of fresh LB medium (WT) or Hopwood minimal media (mutants). Kanamycin was added as selection agent. The cultures were grown in a 15 L fermentor at 37 °C (WT) or 28 °C (mutants) under agitation (400 rpm), in the presence of air (one culture volume per minute)

[1]Abbreviations: LB, Luria−Bertani; IPTG, isopropyl α-D-thiogalactoside; IEF, isoelectrofocusing analysis.

and at constant pH of 6.8. At an A_{600} of 1.6, IPTG (500 μM final concentration) was added, and the cultures were incubated for an additional 5 h. The bacteria were harvested by centrifugation on a Westphalia separator (London, U.K.) and resuspended in 300 mL of 30 mM Tris-HCl buffer, pH 8, 30% sucrose, and 10 mM EDTA. The periplasmic fraction was recovered as follows: lysozyme (final concentration of 0.2 mg/mL) was added to the mixture. After 30 min of incubation at 4 °C, the action of lysozyme was stopped by addition of $CaCl_2$ (20 mM final concentration). The suspension was then centrifuged at 30000*g* for 30 min at 4 °C. The supernatant which contained the periplasmic fraction was collected and dialyzed twice against 15 L of 20 mM Tris-HCl, pH 8.6, buffer (buffer A) at 4 °C. The solution was loaded on a QAE-Sepharose Fast Flow column (150 mL, 2.6 × 40 cm; Amersham Biosciences) equilibrated in buffer A. The gel was washed by 10 volumes of buffer A at a flow rate of 5 mL/min. The β-lactamase was eluted at a rate of 5 mL/min using a linear salt gradient (0−300 mM NaCl) made in 10 column volumes of buffer A. The active fractions were collected, pooled, and dialyzed twice against 12 L of buffer A. The solution was loaded on a Source 15Q column (20 mL, 1.6 × 9.5 cm; Amersham Biosciences) equilibrated in buffer A. The β-lactamase was eluted at a flow rate of 2 mL/min using a linear NaCl gradient (0−200 mM) of 12 column volumes in buffer A. The protein sample was finally dialyzed twice against buffer A to bring the Cl^- concentration below 1 μM and avoid any inhibition. The purity of the different proteins was over 98%. Final concentrations of the different enzymes were determined by measuring absorbance at 280 nm and using the theoretical extinction coefficient of 47630 $M^{-1}\cdot cm^{-1}$ (WT) or 41940 $M^{-1}\cdot cm^{-1}$ (mutants). The molecular masses of all purified proteins were confirmed by electrospray mass spectrometry. The protein samples (100 pmol) were dissolved in formic acid/acetonitrile (1:1000 v/v) in water and injected with a syringe pump (Harvard Instruments, South Natick, MA) at a flow rate of 6 μL/min into the source of the mass spectrometer VG BioQ upgraded with a Platform source (Micromass, Altrincham, Cheshire, U.K.).

Isoelectrofocusing Analysis (*IEF*). Isoelectric points (p*I*) of purified WT and mutants of OXA-10 β-lactamases were determined by IEF electrophoresis using Ampholin PAGplates, pH gradient 3−9.5, in a Multiphor II electrophoresis system apparatus (Amersham Biosciences, Uppsala, Sweden) for 2.5 h at 25 W, 25 mA, and 2000 V. β-Lactamase activity was revealed with nitrocefin (100 μM).

N-Terminal Sequencing. N-Terminal sequences of the different purified proteins (10−50 pmol) were performed by Edman degradation on a Procise protein sequencing system equipment (Applied Biosystems, London, England).

Differential Scanning Calorimetry. Measurements were performed using a MicroCal VP-DSC (MicroCal, London, England) instrument at a scan rate of 1 °C/min from 20 to 80 °C. Samples were dialyzed overnight against 50 mM phosphate buffer, pH 7, complemented or not by 50 mM $NaHCO_3$ (870 or 19.2 μM CO_2), the latter being used in the reference cell for the determination of the buffer baseline. Protein concentrations (13 μM) were determined after dialysis by the bicinchoninic acid protein assay reagent (Pierce, Rockford, IL). Thermograms of the different OXA-10 β-lactamases were analyzed according to a single non-two-state transition model in which $T_{1/2}$ and ΔH_{cal} were fitted independently using the MicroCal Origin 5 software. Curves were adjusted with SigmaPlot 8.0.

Molecular Sieves. The apparent molecular masses of the different proteins were measured as follows. β-Lactamase solutions (18 μM) were prepared in 50 mM phosphate, pH 7, buffer in the absence or in the presence of 50 mM $NaHCO_3$ (19.2 or 870 μM CO_2). The different samples (500 μL) were loaded on a Superdex HR 10/30 molecular sieve column equilibrated with 50 mM phosphate buffer, pH 7, containing or not 50 mM $NaHCO_3$. The protein elution was realized at a 1 mL/min flow rate. The column was previously calibrated with bovine serum albumin (BSA) (M_r = 66000 Da) and the TEM-1 β-lactamase (M_r = 29000 Da). The elution volumes of the different proteins were determined by recording A^{280} values.

Kinetic Parameters. All of the kinetics measurements were performed at 25 °C in 50 mM phosphate buffer, pH 7, containing or not 50 mM $NaHCO_3$ (870 or 19.2 μM CO_2). The variation of absorbance of the substrate solution was measured on a double beam Uvikon XL spectrophotometer. The steady-state kinetic parameters were determined from the initial rates using both the Hanes−Wolf linearization of the Henri Michaelis−Menten equation and a direct nonlinear regression with the hyperbolic equation using the SigmaPlot program. Activation of the W154F mutant by CO_2 was conducted as follows. The W154F mutant (4 μM final concentration) was incubated in the presence of nitrocefin (100 μM) in 50 mM phosphate buffer, pH 7. When the reaction reached the steady state, a solution of $NaHCO_3$ (50 mM final concentration) was added, and the rate of hydrolysis of the substrate was monitored.

The pH dependence of the steady-state kinetic parameters (k_{cat}, K_M, and k_{cat}/K_M) was measured by analyzing the complete hydrolysis time courses (*39*) of cephalothin (25−100 μM) from pH 6 to pH 10 at 25 °C in two different polybuffers (buffer 1, acetate, MES, MOPS, CHES, and HEPES; buffer 2, acetate, MES, and Tris; 50 mM of each) complemented or not with 50 mM sodium bicarbonate (870 or 19.2 μM CO_2). The ionic strength of the two polybuffers are respectively 250 and 150 mM.

Apparent Dissociation Constant (K_D^{app}) *for* CO_2. For the wild type and the W154H mutant, the apparent dissociation constant (K_D^{app}) of the carboxylated lysine versus free lysine and CO_2 was determined using benzylpenicillin as described by Golemi et al. (*21*). For W154G, W154A, and W154F, all of the working solutions and the spectrophotometer were introduced in a CO_2-free glovebox (Jacomex, France) saturated by nitrogen gas. The hydrolysis rate of nitrocefin (200 μM) by the different β-lactamases (5 μM) was measured as a function of the concentration of sodium bicarbonate (0−50 mM; 0−870 μM CO_2) in a 100 mM phosphate buffer, pH 7.5, with an Ocean optics fiber spectrophotometer. Two types of curves, sigmoid and hyperbolic, were observed. In the case of the wild-type enzyme and W154H, the apparent dissociation constant K_D^{app} was calculated with the help of eq 1, where RA and [CO_2] are the residual activity and the concentration of carbon dioxide, respectively.

$$RA = \frac{[CO_2]}{K_D^{app} + [CO_2]} \quad (1)$$

In the case of the W154G, W154A, and W154F OXA-10 mutants, the K_D^{app} values were obtained from eq 2, where *n* is the Hill coefficient describing the cooperativity between binding sites.

$$RA = \frac{[CO_2]^n}{K_D^{app} + [CO_2]^n} \quad (2)$$

X-ray Crystallography. The crystals of the Trp154 mutants of the OXA-10 enzyme were obtained at 20 °C by the hanging

Table 1: Crystallographic Data and Refinement Statistics[a]

	W154A	W154G	W154H	W154A-PenG
Diffraction Data Statistics				
space group	$P2_12_12_1$	$P2_1$	$P2_12_12_1$	$P2_12_12_1$
unit cell parameters				
a, b, c (Å)	48.6, 96.72, 125.55	47.11, 125.4, 92.36	48.68, 97.06, 125.68	48.80, 93.10, 127.70
α, β, γ (deg)	90, 90, 90	90, 99.8, 90	90, 90, 90	90, 90, 90
resolution range (Å)	19.4− 2.2 (2.32−2.2)	46.47−2.7 (2.85−2.7)	48.68−1.9 (2.00−1.9)	48.57−2.8 (3.0−2.85)
unique reflections	30362	28824	47547	14053
completeness (%)	98.7 (97.9)	99.2 (99.3)	99.4 (96.2)	99.0 (99.8)
redundancy	7.2 (7.3)	3.3 (3.2)	5.3 (3.5)	6.9 (6.5)
R_{merge} (%)[b]	13.0 (40.1)	12.2 (45.2)	12.3 (76.2)	12.4 (68.1)
average I/σ	15.1 (5.5)	11.0 (3.1)	10.9 (1.7)	15.1 (3.0)
Refinement Statistics				
resolution range (Å)	19.4−2.2 (2.26−2.2)	44.54−2.7 (2.77−2.7)	48.68−1.9 (1.95−1.9)	13.65−2.85 (2.92−2.85)
no. of reflections	28742 (2056)	27307 (2019)	45064 (3069)	13300 (924)
R_{factor} (%)[c]	16.8 (18.2)	21 (32.2)	16.9 (25.4)	19.5 (30.6)
R_{free} (%)[d]	21.1 (23.8)	26.7 (37.7)	21.8 (32.0)	26.2 (36.8)
rms deviations				
bond length (Å)	0.011	0.007	0.015	0.012
bond angles (deg)	1.298	1.075	1.497	1.490
no. of atoms, protein/solvent/ligand	3860/347	7475/147	3924/424	3785/38/46
B-factor, protein/solvent/ligand	23.4/33.7	32.7/20.5	26.8/36.9	39.9/37.9/42.6

[a]Values in parentheses correspond to the high-resolution shell. [b]$R_{merge} = \sum(I - \langle I\rangle)/\sum I$; I is the intensity of an individual reflection and $\langle I\rangle$ the mean value of all the measurements of that reflection. [c]$R_{factor} = \sum|F_o - F_c|/\sum|F_o|$; F_o and F_c are respectively the observed and calculated structure factors. [d]R_{free} calculated for a randomly selected subset of reflections (5%) that were omitted during the refinement.

drop vapor diffusion method under conditions similar to those used for the wild-type enzyme. The W154A mutant (11 mg/mL) crystallized in the presence of various concentrations of $(NH_4)_2SO_4$ (between 1.6 and 2.2 M) in a 0.1 M HEPES, pH 7.5, buffer. Crystals of the W154G mutant (7.9 mg/mL) were obtained in 2.2 M $(NH_4)_2SO_4$ and 0.1 M HEPES, pH 7.0, with 10 mM betaine as additive. The best crystals of the W154H mutant (12 mg/mL) were obtained in the same buffer by lowering the $(NH_4)_2SO_4$ concentration to 1.6 M and adding 30% ethylene glycol.

The crystals of the W154A and W154H mutants grew as large prisms and belong to the orthorhombic space group $P2_12_12_1$ like the native enzyme crystals (PDB ID: 1K4F), with similar unit cell parameters (Table 1). The asymmetric unit contains two molecules forming a biological dimer. The crystals of the W154G mutant appeared as long needles and belonged to the space group $P2_1$ with different unit cell dimensions (Table 1). The asymmetric unit contains four molecules corresponding to two biological dimers. The solvent content of the three mutants' crystals is about 50%. The W154A-PenG complex was obtained by soaking a crystal for 2 h in a solution containing 2.2 M $(NH_4)_2SO_4$, 0.1 M MES, pH 6, and 100 mM benzylpenicillin.

X-ray diffraction experiments were carried out under cryogenic conditions (100 K) after transferring the crystals into a reservoir solution supplemented with 50% glycerol. The diffraction data related to the crystals of the W154A mutant and the complex between this mutant and benzylpenicillin (W154A-PenG) were collected with a Rigaku RU-200 rotating anode generator operating at 40 kV and 100 mA and a Marresearch Mar345 imaging plate (λ = 1.5418 Å). Data for the W154G and W154H mutants were measured at the ESRF synchrotron (Grenoble, France) on the FIP-BM30a beamline (λ = 1.0 and 0.978872 Å, respectively) using a Marresearch 165 mm CCD and an ADSC QUANTUM 315 detector, respectively. All of the data were indexed and integrated using the XDS software (*40*). The scaling and reducing steps were performed using the SCALA and TRUNCATE modules of the CCP4 package (*41*). Data collection statistics are shown in Table 1.

A molecular replacement solution was obtained for each crystal using the program AMoRe (*42*) with the structure of the wild-type OXA-10 enzyme (PDB ID: 1K4F) as search model. The final four structures were then obtained after a few cycles of refinement with the program Refmac 5.2 (*43*) and model building with the program COOT (*44*). The verification of the mutated residues was carried out using a combination of omit maps and difference maps. The R_{factor} and R_{free} values are summarized in Table 1. Figures were generated with PYMOL (*45*). The data and refinement statistics related to the W154A mutant at pH 6.0 and 9.0 are presented as Supporting Information (Table S2).

RESULTS

Production and Purification. Compared to the wild-type enzyme, which was produced at more than 60 mg/L in LB medium at 37 °C, W154 mutants were produced in Hopwood minimum medium at 28 °C with a yield of 3−4 mg/L. The purification yield of the mutants never exceeded 45% with a degree of purity of 98% (data not shown). The purification yields of the WT and W154H mutant enzymes were 80% with degrees of purity of 99%. The N-terminal sequences of the different mutants (NH_2-MGSIT) were in agreement with the wild-type N-terminal sequence, and mass spectrometry confirms the masses of the different mutants. The pI of the W154 OXA-10 mutants (pI = 7.7) were one pH unit higher than that of the OXA-10 WT (pI = 6.6). Nevertheless, mutants interacted strongly with the QAE-Sepharose gel at pH 8,6.

Molecular Sieve Chromatography. The elution volume ($v_e \approx$ 10−10.5 mL) of the different OXA-10 β-lactamases

Table 2: Apparent Melting Temperatures ($T_{1/2}$) and Calorimetric Enthalpies (ΔH_{cal}) for the Different OXA-10 β-Lactamases in 50 mM Phosphate Buffer, pH 7, in the Presence of 1.1 mM (19.2 μM CO_2) or 50 mM (870 μM CO_2) Sodium Bicarbonate

		OXA-10			
	$[CO_2]$ (μM)	WT	W154G	W154A	W154F
$T_{1/2}$ (°C)	≤19.2	55.9 ± 0.05	41.9 ± 0.07	39.9 ± 0.05	48.8 ± 0.05
	870	60 ± 0.07	50.7 ± 0.04	56.7 ± 0.05	53.5 ± 0.07
ΔH_{cal} (kcal mol^{-1})	≤19.2	109 ± 0.6	78 ± 0.7	90 ± 0.5	122 ± 0.4
	870	137 ± 0.1	94 ± 0.5	85 ± 0.4	110 ± 0.3

indicated that the proteins were dimeric. We also noted that v_e's (10−10.2 mL) of the mutants were slightly smaller than that of the WT enzyme (10.4 mL). This phenomenon could be at least partially related to an increase of the Ω-loop mobility in the absence of the Trp154 side chain inducing a larger Stokes radius of the mutants. Our experiments also indicated that addition of 50 mM sodium bicarbonate (870 μM CO_2) slightly increased the value of v_e by ± 0.1 mL, which suggests a more compact protein. This effect could be the result of a more carboxylated Lys70 preventing a more flexible conformation of the 89−107 and 115−118 loops observed in some OXA-10 crystallographic structures solved below pH 7.5 where Lys70 is not carboxylated (*21*).

Differential Scanning Calorimetry (*DSC*). The thermograms for the thermal denaturation of wild type and mutants OXA-10 in 50 mM phosphate buffer, pH 7, exhibited a single transition temperature in an irreversible process. Therefore, we only determined the half-denaturation temperature ($T_{1/2}$) and the total heat absorption (ΔH_{cal}) necessary to yield an unfolded protein (Table 2 and Supporting Information Figure S1). As aggregation was only apparent at high temperature ($T > T_{1/2}$), we assumed that this phenomenon slightly affected the $T_{1/2}$ and ΔH_{cal} values. Substitution of Trp154 induced a decreased stability of the protein which was reflected in a shift of $T_{1/2}$ from 55.9 to 39.9−41.9 °C depending of the mutant. The presence of CO_2 resulted in an enhanced stability of the β-lactamase. For example, $T_{1/2}$ of W154A shifted from 39.9 to 56.7 °C. The value of the calorimetric enthalpy (ΔH_{cal}) showed that the wild-type enzyme and the W154F were the most stable proteins at low or high sodium bicarbonate concentration. The measurements confirmed also that W154G was the least stable protein.

Kinetic Parameters. Substitution of the Trp154 residue by glycine, alanine, phenylalanine, and histidine significantly affected the kinetic steady-state parameters (table 3). In the absence of added sodium bicarbonate, W154G and W154A are the mutants with the most affected catalytic efficiency (30−22000-fold lower) driven by a decrease of 200−12000-fold of k_{cat} and an increase of K_M values by factors of 2−10. In the case of the W154H mutant, K_M values were in the range of those of the W154G and W154A mutants, but we observed a 3−300-fold increase of the k_{cat} values. These values are however still at least 25 times lower than the WT ones. For the W154F mutant, no catalytic parameters could be recorded due to a time-dependent inactivation of the enzyme.

Addition of 50 mM $NaHCO_3$ induced activation of the different mutants as well as of the WT OXA-10. As already mentioned by Golemi et al. (*21*), at low bicarbonate concentration, the OXA-10 enzyme exhibited biphasic kinetics for all tested substrate except benzylpenicillin and cephalothin. The same phenomenon was observed for the W154G, W154A, and W154H OXA-10 mutants. In the presence of added $NaHCO_3$ as a source of carbon dioxide, the kinetics were apparently monophasic except for cloxacillin and oxacillin. For the mutants, addition of $NaHCO_3$ induced a significant improvement of the catalytic efficiency driven by a decrease of K_M values (2−20-fold) and an increase of k_{cat} values (2−200-fold). This effect was even more significant for the W154F mutant for which the inactivation observed at a low sodium bicarbonate concentration was reversed (Figure 1). In these conditions, the catalytic parameters of the W154F mutant are similar to those of the W154H mutant except for cephalothin which is hydrolyzed with the same efficiency by W154F and the WT enzymes.

We determined the pH dependence of the WT and W154H catalytic parameters with two different buffers (Figure 2). The WT enzyme has a maximum k_{cat} value around pH 9, but the highest catalytic efficiency is between pH 6 and pH 7 due to the increased K_M values at higher pH. For the W154H mutant, the maximum of activity (k_{cat}) is shifted by about 2 units toward the lower pH. In buffer 2, we observed a small increase of the catalytic efficiency of the WT OXA-10 at pH 9 and 10 due to a slight decrease of the K_M. No significant effect of the nature of the buffer is seen with the W154H mutant. The presence of 50 mM sodium bicarbonate did not significantly affect the different pH profiles (Supporting Information Figure S2).

Apparent CO_2 Dissociation Constants. Since carbon dioxide is an activator of class D β-lactamase, we calculated its apparent dissociation constant for the different enzymes. The measure of the normalized substrate hydrolysis by the different proteins has been performed with increasing concentration of dissolved carbon dioxide and different enzyme concentrations imposed by the individual catalytic activity of each protein. Knowing that the dissociation constant of the dimer is estimated at 1 μM (*21*), we assumed that, in our working conditions, W154G, W154A, and W154F OXA-10 were dimeric. On the other hand, the WT and W154H enzymes were used at concentrations below 100 nM and were thus predominantly in the monomeric forms. This corresponds to a hyperbolic curve (Figure 3) and reflects a Hill coefficient of 1, implying a single binding site. On the opposite, sigmoid curves are observed for the W154G, W154A, and W154F mutants. In the case of the W154F mutant, the Hill coefficient is equal to 2.0, which indicates a positive cooperative in the binding of carbon dioxide. However, for the W154G and W154A mutants, the experimental data did not allow a relevant measurement of the Hill coefficient. Substitution of Trp154 by glycine, alanine, or phenylalanine yielded a large increase of the K_D^{app} constant (104 ± 5, 85 ± 5, and 80 ± 6 μM for W154G, W154A, and W154F, respectively) compared to the wild-type enzyme (13 ± 2.5 μM, which is similar to that of Golemi et al. (*21*)). On the opposite, the W154H mutant was characterized by a K_D^{app} value of 18 ± 3 μM, which is similar to that of the wild type. These experiments were also performed with another cephalosporin substrate

Table 3: Kinetic Parameters of the W154G, W154A, W154F, and OXA-10 Enzymes Measured in the Presence of 1.1 mM (19.2 μM CO_2) or 50 mM (870 μM CO_2) Sodium Bicarbonate[a]

		[CO_2] = 19 μM			[CO_2] = 870 μM		
OXA-10	antibiotic	k_{cat} (s^{-1})	K_M (μM)	k_{cat}/K_M (M^{-1} s^{-1})	k_{cat} (s^{-1})	K_M (μM)	k_{cat}/K_M (M^{-1} s^{-1})
W154G	benzylpenicillin	$(4 \pm 0.4) \times 10^{-2}$	600 ± 140	67 ± 17	0.13 ± 0.002	10 ± 4	$(1.3 \pm 0.5) \times 10^4$
	ampicillin	$(1.26 \pm 0.04) \times 10^{-2}$*	230 ± 10*	56 ± 2*	0.132 ± 0.004	40 ± 10	$(3.3 \pm 0.8) \times 10^3$
	cloxacillin	2.5 ± 0.3*	220 ± 80*	$(1.3 \pm 0.4) \times 10^4$*	3.5 ± 0.2	200 ± 50	$(1.8 \pm 0.4) \times 10^4$
	oxacillin	3.5 ± 0.001*	200 ± 4*	$(1.75 \pm 0.3) \times 10^4$*	4 ± 0.2	100 ± 20	$(4 \pm 0.8) \times 10^4$
	cephaloridine	$(3.6 \pm 0.4) \times 10^{-3}$*	290 ± 40*	12 ± 2*	$(2 \pm 0.1) \times 10^{-3}$	65 ± 10	30 ± 5
	cephalothin	$(2.3 \pm 0.3) \times 10^{-3}$	450 ± 30	5 ± 0.3	$(3 \pm 0.3) \times 10^{-3}$	210 ± 40	14 ± 3
	nitrocefin	4 ± 0.3*	100 ± 20*	$(4 \pm 0.8) \times 10^4$*	8 ± 1	60 ± 5	$(1.3 \pm 0.2) \times 10^5$
W154A	benzylpenicillin	$(8 \pm 0.8) \times 10^{-2}$	150 ± 30	530 ± 120	0.7 ± 0.2	60 ± 10	$(1.2 \pm 0.4) \times 10^4$
	ampicillin	$(7 \pm 0.2) \times 10^{-2}$*	60 ± 10*	$(1.15 \pm 0.2) \times 10^3$*	1.4 ± 0.3	30 ± 5	$(4.7 \pm 1.2) \times 10^4$
	cloxacillin	0.2 ± 0.03*	100 ± 15*	$(2 \pm 0.4) \times 10^3$*	4 ± 0.2	30 ± 5	$(1.3 \pm 0.2) \times 10^5$
	oxacillin	0.25 ± 0.03*	60 ± 15*	$(4.2 \pm 1) \times 10^3$	4.5 ± 0.3	20 ± 5	$(2.3 \pm 0.6) \times 10^4$
	cephaloridine	$(4 \pm 0.4) \times 10^{-3}$*	450 ± 100*	10 ± 2*	$(1.5 \pm 0.2) \times 10^{-2}$	60 ± 15	250 ± 70
	cephalothin	$(3 \pm 0.2) \times 10^{-3}$	210 ± 40	14 ± 3	$(1.2 \pm 0.2) \times 10^{-2}$	40 ± 5	300 ± 60
	nitrocefin	0.6 ± 0.02*	110 ± 20*	$(5.5 \pm 1) \times 10^3$*	6 ± 0.5	35 ± 5	$(1.7 \pm 0.2) \times 10^5$
W154F	benzylpenicillin		inactivation		2.5 ± 0.1	100 ± 20	$(2.5 \pm 0.5) \times 10^4$
	ampicillin		inactivation		2.4 ± 0.1	125 ± 20	$(1.9 \pm 0.3) \times 10^4$
	cloxacillin		inactivation		1.8 ± 0.2	140 ± 10	$(1.2 \pm 0.2) \times 10^4$
	oxacillin		inactivation		2 ± 0.2	125 ± 10	$(1.6 \pm 0.2) \times 10^4$
	cephaloridine		inactivation		1.3 ± 0.2	50 ± 8	$(2.6 \pm 0.6) \times 10^4$
	cephalothin		inactivation		8 ± 0.5	25 ± 5	$(3.2 \pm 0.6) \times 10^5$
	nitrocefin		inactivation		2 ± 0.1	50 ± 8	$(3 \pm 0.6) \times 10^4$
W154H	benzylpenicillin	1.5 ± 0.5	17 ± 10	$(8 \pm 0.6) \times 10^4$	4 ± 0.4	70 ± 15	$(5.7 \pm 1.3) \times 10^4$
	ampicillin	3 ± 1*	250 ± 50*	$(1.3 \pm 0.5) \times 10^4$*	18 ± 2	150 ± 30	$(1.2 \pm 0.3) \times 10^5$
	oxacillin	35 ± 10*	650 ± 100*	$(5.3 \pm 1.5) \times 10^4$*	90 ± 6	130 ± 15	$(7 \pm 0.9) \times 10^5$
	cephalothin	$(1 \pm 0.1) \times 10^{-1}$*	5 ± 0.5*	$(2 \pm 0.4) \times 10^4$*	$(1.5 \pm 0.2) \times 10^{-1}$	4 ± 1	$(3.5 \pm 0.9) \times 10^4$
	nitrocefin	1 ± 0.2*	10 ± 4*	$(1 \pm 0.4) \times 10^5$*	2.5 ± 0.3	13 ± 2	$(1.9 \pm 0.3) \times 10^5$
WT	benzylpenicillin	85 ± 10	55 ± 6	$(1.5 \pm 0.4) \times 10^6$	120 ± 10	20 ± 1	$(6.0 \pm 0.6) \times 10^6$
	ampicillin	160 ± 90*	180 ± 30*	$(0.9 \pm 0.5) \times 10^6$*	220 ± 20	35 ± 5	$(6.2 \pm 0.1) \times 10^6$
	cloxacillin	500 ± 30*	250 ± 30*	$(2 \pm 0.3) \times 10^6$*	120 ± 10*	110 ± 10*	$(1 \pm 0.1) \times 10^6$*
	oxacillin	600 ± 20*	200 ± 20*	$(3 \pm 0.3) \times 10^6$*	300 ± 10*	100 ± 20*	$(3 \pm 0.6) \times 10^6$*
	cephaloridine	35 ± 10*	$(2 \pm 0.8) \times 10^3$*	$(1.8 \pm 0.8) \times 10^4$*	70 ± 20	400 ± 100	$(1.8 \pm 0.6) \times 10^5$
	cephalothin	2.0 ± 0.2	5 ± 0.6	$(4 \pm 0.7) \times 10^5$	2.5 ± 0.1	7 ± 1	$(3.8 \pm 0.5) \times 10^5$
	nitrocefin	1300 ± 50*	25 ± 5*	$(5.2 \pm 1.0) \times 10^7$*	1700 ± 100	10 ± 5	$(1.7 \pm 0.9) \times 10^8$

[a]Hydrolyses characterized by biphasic curves are marked with an asterisk, and the values mentioned are measured at the steady state.

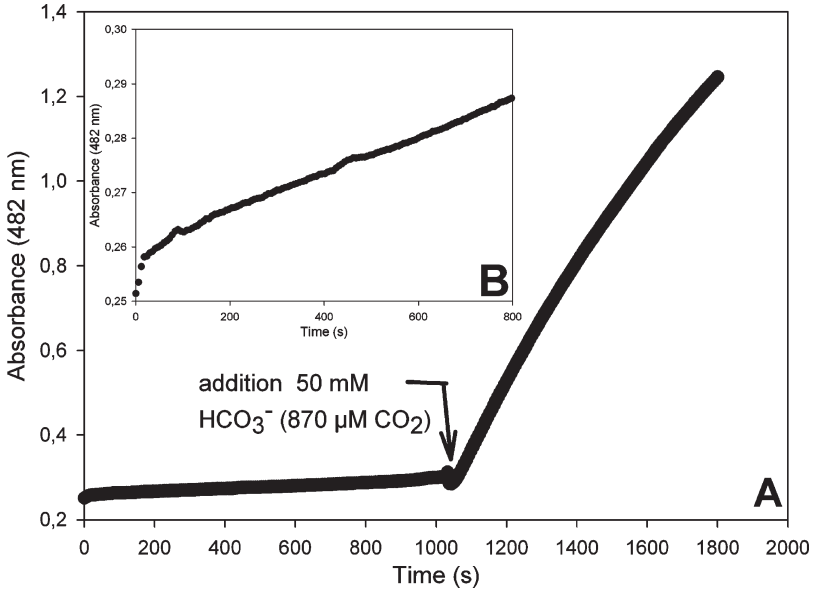

FIGURE 1: Reactivation of the W154F mutant (4 μM) during the hydrolysis of nitrocefin (100 μM) by addition of 50 mM sodium bicarbonate (870 μM CO_2). The different scale used for the inset highlights the variation of the absorbance recorded at the beginning of the experiment.

(cephalothin rather than nitrocefin), and no variation of the K_D^{app} values was observed for the different mutants (data not shown). We may therefore conclude that the choice of substrate does not modify the bicarbonate K_D^{app} values.

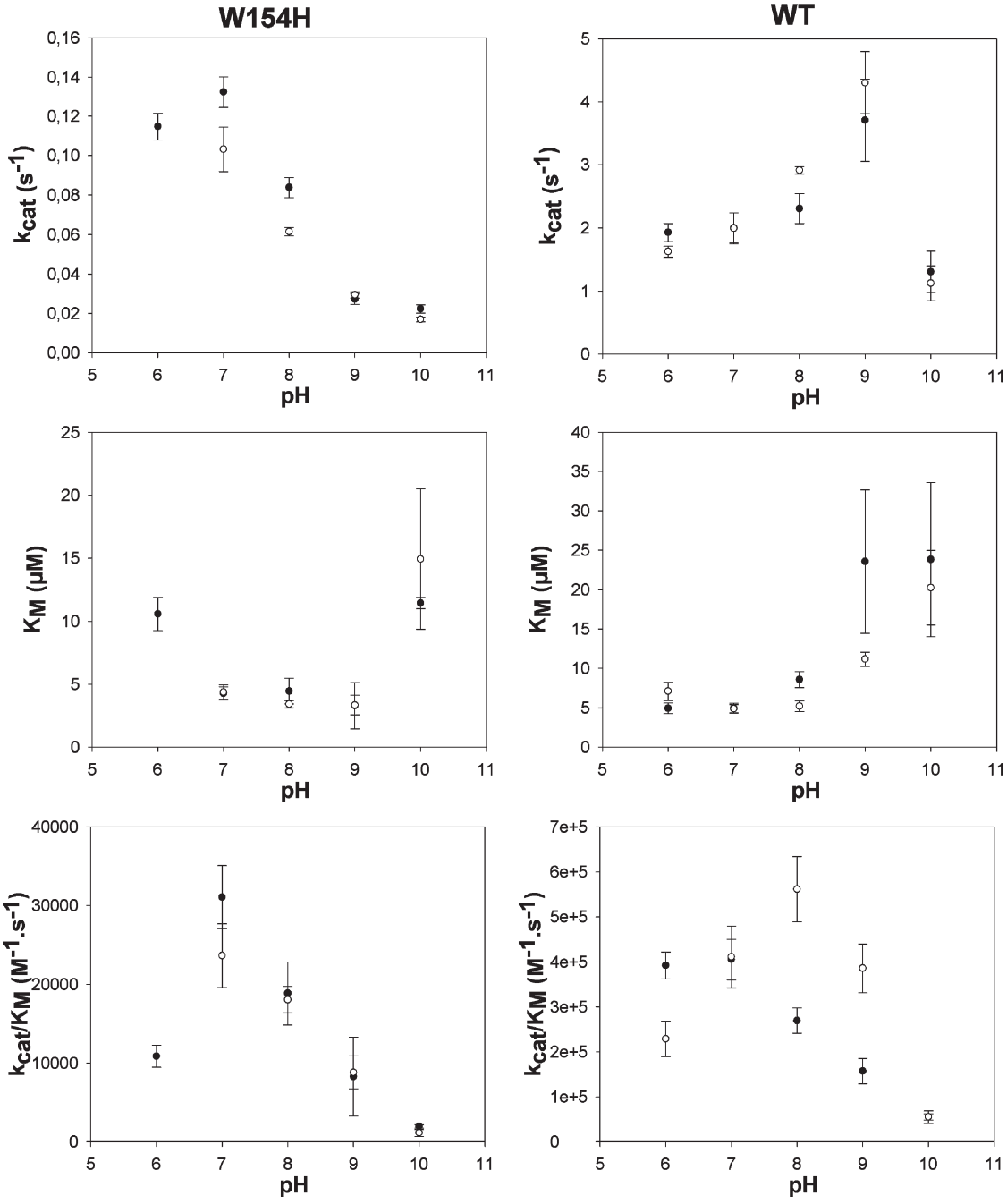

FIGURE 2: pH dependence of the kinetic parameters (k_{cat}, K_M, k_{cat}/K_M) of the W154H mutant and WT enzyme with cephalothin in the presence of 19.2 μM CO_2 for two buffers: acetate, MES, MOPS, CHES, and HEPES (●) or acetate, MES, and Tris (○).

Overall Structure of the OXA-10 W154G/A/H Mutants. In the crystallization conditions, the protein concentration is above 300 μM, and thus the dimeric species is the one observed in the crystals. In the $P2_12_12_1$ space group (WT and W154A and W154H mutants) the asymmetric unit contains one dimer. We will refer to it as the AB dimer. In the $P2_1$ space group (W154G mutant) two dimers compose the asymmetric unit, the AB and CD dimers. The mutations had no major effect on the overall structure of the OXA-10 enzyme (Figure 5A,C,E). When the mutant structures were superimposed to that of the native enzyme, the root-mean-square deviations for the equivalent backbone atoms (N, Cα, C, O) were distributed from 0.19 to 0.76 Å, the smallest deviations being observed between equivalent monomers from the different structures and the largest deviations being observed between the WT enzyme and the W154G mutant. Those values are relatively low, and there is only one significant change observed in the Ω-loop which bears the Trp154 residue and forms the bottom of the active site. The Ω-loop conformation is well conserved in both monomers of the W154A and W154H mutants compared to the WT enzyme (Figure 4A,B,E,F). However, the mutation of Trp154 into a glycine induces an important flexibility of the Ω-loop. The electron density in this region was indeed very poor, and the entire loop could only be built in monomer A. In this case the Cα atom of Trp154 and Gly154 superposed well. In monomers B, C, and D, the Ω-loop has a completely different and mostly disordered conformation that results in a very open active site (Figure 4C,D). The disorder of the Ω-loop in the W154G mutant likely explains the modification of the crystallographic packing and the subsequent space group difference compared to the WT enzyme.

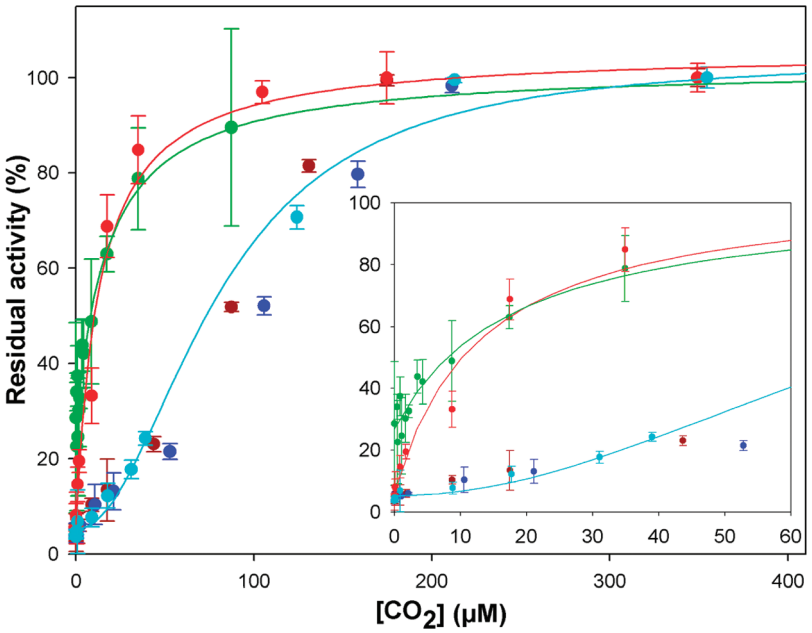

FIGURE 3: Evolution of the residual activity of the WT enzyme (red curve) and the W154A (blue points), W154G (brown points), W154F (cyan curve), and W154H (green curve) mutants in a CO_2-free glovebox with 200 μM nitrocefin or 1 mM benzylpenicillin substrates in degassed 50 mM phosphate buffer, pH 7.5, with increasing concentrations of sodium bicarbonate as source of carbon dioxide. The different scale used for the inset highlights the measurements performed at low CO_2 concentrations.

Active Site Geometry of the OXA-10 W154A/G/H Mutants. In the W154A mutant structure, solved at pH 7.5, the most striking observation is the absence of carboxylation of residue Lys70 in both monomers (Figure 4B). In order to make sure this observation was in relation with the mutation and not with the crystallization pH, we have also solved the structure of the W154A mutant at pH 6.0 and 9.0 (diffraction data and refinement statistics are reported as Supporting Information). A noncarboxylated Lys70 is observed at all pH values. This situation induces a modification in the hydrogen bond network compared to the wild-type enzyme at pH 9. But, even if the interaction of the side chain nitrogen atom of Trp154 is lost, the conformation and orientation of Lys70 and Ser67 in the W154A mutant are the same as in the pH 9.0 WT structure where Lys70 is carboxylated. The hydroxyl group of Ser115 still interacts with the amino group of Lys205, but the distance between the hydroxyl groups of Ser115 and Ser67 increases up to 3.9 Å for monomer A. The oxyanion hole is conserved with a water molecule at hydrogen-bonding distance of the Ser67 and Phe208 main chain nitrogen atoms.

As already described above, the active site of the W154G mutant undergoes more change, especially in the Ω-loop defining its bottom and bearing the Gly154 residue. As a consequence of the low resolution (2.7 Å), electron densities are less defined in some loops. Anyway, a clear electron density defines the residues of the active site, and as in the W154A mutant, Lys70 is clearly not carboxylated in the four monomers (Figure 4D). The position of residues 114−119 is still well conserved, and the orientation of Lys70 is also roughly the same in the four monomers as in the WT and W154A structures. On the opposite, the amino group of the side chain of Lys70 interacts more loosely with the hydroxyl group of Ser67. The situation is different in each monomer, and the distance between Lys70-Nζ and Ser67-Oγ varies from 2.7 to 5.0 Å for monomers D and B, respectively. The hydroxyl group of Ser115 still interacts with the amino group of Lys205, but the distance between the hydroxyl groups of Ser115 and Ser67 varies in each monomer. No water molecule is observed in the oxyanion hole. With all reserve due to the relatively low resolution, we may conclude that the Gly154 mutation induces a very loose hydrogen bond network which leads to a quasi-erratic positioning of the catalytic Ser67, in addition to the noncarboxylation of Lys70.

In the W154H mutant structure, solved at pH 7, the situation observed in monomer B is the same as that described for both monomers of the W154A mutant, where a noncarboxylated Lys70 prevails. The amino group of the side chain of Lys70 interacts with the hydroxyl group of Ser67 and a water molecule. This water molecule is at equal distance to the His154-Nε and somehow mimics the position of the carboxyl group of a carboxylated Lys70. On the other hand, in the active site of monomer A, Lys70 was modeled as partially carboxylated, with 30% for the carboxylated form (Figure 4F). The ε-amino group of noncarboxylated Lys70 interacts with the hydroxyl group of Ser67 and a water molecule as in monomer B. The carboxyl group of the carboxylated form is at hydrogen-bonding distance from the side chain nitrogen atom of His154, the hydroxyl group of the active Ser67, and a water molecule bound to Asn73. The hydroxyl group of Ser115 interacts with the amino group of Lys205, and the oxyanion hole is filled with a conserved water molecule.

Structure of the OXA-10 W154A Mutant in Complex with Benzylpenicillin. The structure of the W154A-PenG complex was determined at a 2.85 Å resolution. Lys70 is not carboxylated, and a clear density is observed for the benzylpenicillin molecules which acylated Ser67 in both monomers. The overall position of the antibiotic is similar to the one usually observed in β-lactamase complexes (Figure 5). The carbonyl oxygen of the former β-lactam ring is in the oxyanion hole, and the phenyl of the 6β side chain is oriented toward the bottom of the active site between Ala98 and Met99 on the left and Phe208 and Gly210 on the right. The thiazolidine ring is located in the upper part of the active site, and two orientations differing by a 15° rotation are found in the two monomers. In monomer B,

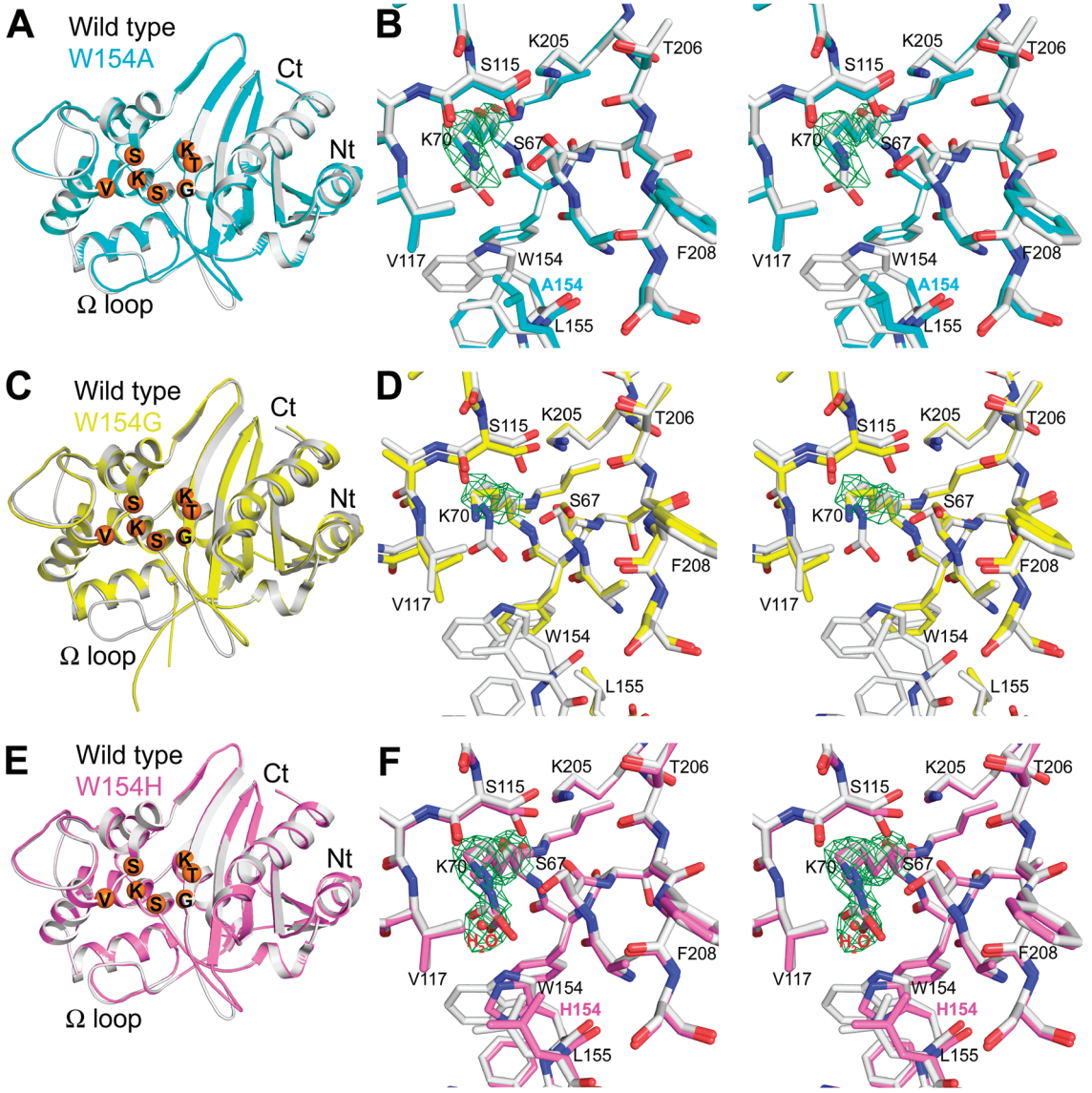

FIGURE 4: Structures of the Trp154 mutants of OXA-10. (A), (C), and (E) are ribbon representations of the W154A (cyan), W154G (yellow), and W154H (magenta) mutants superimposed onto the wild-type OXA-10 structure (light gray). Characteristic residues of the three conserved motifs (SXXK, SXV, and KTG) appear as orange spheres. (B), (D), and (F) are stereographic views of the corresponding superimposed active sites. Omit maps calculated in the absence of the Lys70 residues are shown in green at a 3σ level.

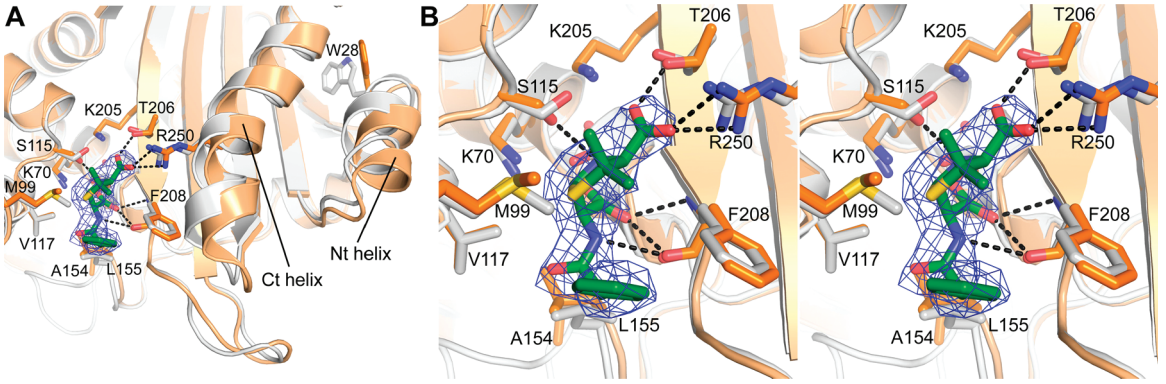

FIGURE 5: Ribbon representation of the superposed structures of the W154-PenG complex (orange) and the W154A mutant at pH 6 (gray). The benzylpenicillin molecule acylated to Ser67 is shown as green sticks, and an omit map calculated in the absence of substrate molecules is displayed in blue at a 2.5σ level.

the carboxyl group attached to the thiazolidine ring interacts solely with the Arg250 side chain while in monomer A it is also involved in a hydrogen bond with the Thr206 side chain. In this conformation, Arg250 is pushed 0.5 Å backward, which is correlated with a 0.75 Å displacement of the C-terminal helix and a 180° rotation of the Trp28 side chain that induces

a subsequent 1.5 Å shift of the N-terminal helix (Figure 5). The structure of the W154A mutant at pH 6 obtained in the same conditions displays none of these changes. They are therefore clearly due to the presence of the benzylpenicillin, but their magnitude has to be taken carefully because of the relatively low resolution.

Acylation of Ser67 of monomer A also leads to a disordered Ω-loop (residues 144−153 are missing in the structure) and a slightly different conformation of the loop following the third conserved motif.

DISCUSSION

Different studies have demonstrated that reactions of CO_2 with α- and ε-amino groups are not rare and that unprotonated amino groups may appear carboxylated in equilibrium with free amino acids and CO_2 (*46*). NMR studies have shown that about 2% of the internal lysine residue is carboxylated in insulin at pH 8.2 in the presence of a physiological concentration of sodium carbonate (*47*). In the case of the class C β-lactamase of *Enterobacter cloacae* P99, the carboxylation of the amine group of some β-lactam antibiotics in bicarbonate containing buffer was also shown to promote a nucleophilic attack of the acyl-enzyme by the formed carbamate, providing an example of an enzymatic catalysis assisted by substrate carboxylation (*48*). Carboxylation of an amine group is pH dependent and will always be a compromise between its deprotonation, favored by high pH, and the concentration of dissolved CO_2, favored by low pH.

In most X-ray structures where a carboxylated lysine has been observed, the modified residue is one of the ligands of a catalytic divalent metal ion. There are only two exceptions, the alanine racemase (*35*) and the class D β-lactamase where the carboxylated lysine is directly involved in the catalytic activity of the enzyme. In the case of alanine racemase, an arginine residue (Arg136) has a role in maintaining the structural integrity of the carboxylate binding site. Its precise positioning is thus of importance in both substrate binding and catalysis (*35*). Arg136 is supposed to promote the deprotonation of the lysine residue (Lys129) which lies in its vicinity. When carboxylated, Lys129 is stabilized by interactions with the side chain atoms of Arg136, the backbone amide and carbonyl of Leu137, and two water molecules. Those interactions determine precisely the position of Arg136. In the case of the OXA-10 β-lactamase, the vicinity of hydrophobic residues (Met99, Trp102, Val117, Leu155, Trp154, and Phe208) is supposed to promote the deprotonation of Lys70, which appears fully carboxylated at high pH in the WT structures. The role of Trp154 is clearly to stabilize the carboxylated Lys70, in a manner similar to the way Arg136 stabilizes the carboxylated Lys129 in alanine racemase.

In OXA-10, the carboxylated Lys70 interacts strongly with the hydroxyl side chain of Ser67 and a water molecule. In the W154G/A mutant structures, when the hydrophobic side chain is absent and the possibility of an interaction with the side chain Nε atom is lost, Lys70 appears as noncarboxylated in both monomers of the biological dimer. The side chain Nζ atom of Lys70 still interacts with a water molecule, but its interaction with Ser67-Oγ seems less strong. It is observed in both mutants, but especially in W154G, that the side chain hydroxyl of Ser67 is not fixed anymore. We may correlate this inefficient positioning of the active serine with the drastic global loss of catalytic efficacy.

The situation of the W154H mutant structure reflects a less dramatic modification with a partially carboxylated Lys70 in monomer A. In this case, the Nε2 nitrogen atom of the His154 imidazole ring is within hydrogen-bonding distance from an oxygen atom of the modified lysine carboxyl group. The second nitrogen of the His154 side chain (Nδ1) cannot get close enough to the carboxylated Lys70 to play a similar role because of the geometry observed in this structure. Therefore, this histidine has to be protonated for the Nε2 nitrogen to act as a hydrogen bond donor similar to that of the nitrogen atom of the indole group of Trp154. So at pH 7, at least a low percentage of the active sites is in a fully active conformation with a protonated His154, which is in a good agreement with the lesser impact of this mutation on the catalytic activity and apparent CO_2 dissociation constant K_D^{app} value. According to this structure, the shift of the optimum catalytic constant (k_{cat}) toward lower pH observed for the W154H mutant when compared to the WT enzyme could be explained by the progressive deprotonation of the histidine, preventing the formation of the hydrogen bond stabilizing the carboxylated Lys70.

On the other hand, the K_D^{app} increased strongly for W154G/A/F mutants compared to the wild-type enzyme. The substitution of Trp154 by a glycine, alanine, or phenylalanine still maintains the hydrophobic character of the side chain but abolishes any possible interaction with a carboxylated Lys70. Those mutations are directly related to the absence or the very poor carboxylation of Lys70 in natural or even in CO_2-supplemented media and to a drastic decrease of the catalytic parameters. Moreover, the presence of a glycine or an alanine in position 154 seems to increase the flexibility of the Ω-loop according to the crystal structures and decrease the overall stability of the enzymes according to the calorimetry experiments.

Globally the poorer substrates are cephaloridine and cephalothin. This is observed for the WT enzyme in natural as well as CO_2-saturated media. This is also true for all mutants with the exception of the W154F mutant which reveals a more peculiar behavior. On the other hand, nitrocefin, a cephalosporin with a bulkier group attached to the cephem ring as single difference, is the most rapidly hydrolyzed antibiotic. From the superposition of a nitrocefin molecule to the W154A-PenG complex we can propose that this 1000-fold activity improvement could be the result of favorable interactions between the hydrogen bond acceptor of the nitrocefin dinitrophenyl group and the Arg250, Lys251, and/or Gln101 side chains present in its vicinity.

The k_{cat} and k_{cat}/K_M for the W154A and W154G mutants decrease drastically for all tested substrates, and we observe a poor increase of catalytic efficiencies with addition of sodium bicarbonate in the medium. In the case of the W154F mutant, an inactivation is observed in natural medium, which is reversed at high concentration of bicarbonate. In this case, the catalytic efficiencies are enhanced in the same way for all tested substrates with no exception.

In the absence of sodium bicarbonate, biphasic kinetics prevail for all substrates, with the exceptions of benzylpenicillin and cephalothin, for the WT enzyme as well as the mutants. However, monophasic kinetics are observed for the four mutants with all substrates in the presence of high sodium bicarbonate concentration. In the case of the WT enzyme, the burst observed with oxacillin and cloxacillin is always present even at high concentration of bicarbonate (*21*). These observations are compatible with the model proposed by Golemi et al. where carboxylated fully active and noncarboxylated mostly inactive enzymes coexist

in solution (*21*). The hydrolysis of the substrate would somehow destabilize the Lys70 carboxylation and shift the equilibrium between these two species toward the non-carboxylated form, explaining the second slower phase of the biphasic kinetics. In the contrary, addition of sodium bicarbonate would prevent this shift and preserve an equilibrium with most of the enzyme in the active carboxylated form and lead to monophasic kinetics.

Interestingly, the OXA-28 β-lactamase differs from OXA-10 by only 10 amino acids, including a replacement of the tryptophan in position 154 by a glycine as the single mutation in close proximity with the active site (*49*). OXA-28 is described as a poorly stable and poorly active enzyme. Its catalytic efficiency against nitrocefin ($k_{cat}/K_M = 1.6\ 10^5\ M^{-1}\ s^{-1}$) is close to that of the single W154G mutant ($k_{cat}/K_M = 4\ 10^4\ M^{-1}\ s^{-1}$). Our data supply a good explanation to the behavior of the OXA-28. The presence of a glycine in position 154 decreases the enzyme stability, increases the flexibility of the Ω-loop, and results in poor activity due to the absence of carboxylation of Lys70.

X-ray structures and apparent CO_2 dissociation constants of the Trp154 mutants also supplied direct information about the carboxylation state of Lys70, as stated above. From the W154A-PenG complex we can conclude that this mutation is at least critical for the deacylation step. Furthermore, the addition of carbon dioxide increases the activity of the different mutants; we can therefore deduce a direct role of the Lys70 carboxylation in the deacylation step consistent with the results obtained for the K70 mutation in OXA-1 (*50*). However, none of the mutants regain the full activity of wild-type OXA-10 in conditions inducing full carboxylation of this lysine including also the W154H mutant which can mimic the stabilizing hydrogen bond observed with Trp154. This means that Trp154 not only promotes and stabilizes the carboxylated form of Lys70 but also favors its optimum orientation which is critical for the positioning of the other catalytic elements in the active site. Indeed, in the absence of Trp154 and the lysine carboxylation, the hydrogen bond network of the active site was significantly altered. The position of the Ω-loop containing Trp154 is therefore also important as confirmed by the Asp66 mutation in OXA-1 where this residue is making a hydrogen bond stabilizing the Ω-loop (*29*).

The fact that the shifts of the N- and C-terminal helices of OXA-10 in the W154A-PenG complex are only observed in monomer A indicates that the crystal packing influences the observed structure. This difference however emphasizes the potential plasticity undergone by the enzyme during the hydrolysis of the substrate.

ACKNOWLEDGMENT

The authors thank Romain Guiet for help during this work.

SUPPORTING INFORMATION AVAILABLE

List of oligonucleotides used during this work (Table S1), crystallographic data and refinement statistics for the W154A mutant at pH 6 and 9 (Table S2), differential scanning calorimetric thermograms of the WT OXA-10, W154G, W154A, and W154F mutants (Figure S1), and pH dependence of the kinetic parameters (k_{cat}, K_M, k_{cat}/K_M) of the W154H mutant and WT enzyme with cephalothin in the presence of 870 μM CO_2 (Figure S2). This material is available free of charge via the Internet at http://pubs.acs.org.

REFERENCES

1. Matagne, A., Dubus, A., Galleni, M., and Frere, J. M. (1999) The beta-lactamase cycle: a tale of selective pressure and bacterial ingenuity. *Nat. Prod. Rep. 16*, 1–19.
2. Ambler, R. P. (1980) The structure of beta-lactamases. *Philos. Trans. R. Soc. London, Ser. B 289*, 321–331.
3. Jaurin, B., and Grundstrom, T. (1981) ampC cephalosporinase of *Escherichia coli* K-12 has a different evolutionary origin from that of beta-lactamases of the penicillinase type. *Proc. Natl. Acad. Sci. U.S.A. 78*, 4897–4901.
4. Dale, J. W., Godwin, D., Mossakowska, D., Stephenson, P., and Wall, S. (1985) Sequence of the OXA2 beta-lactamase: comparison with other penicillin-reactive enzymes. *FEBS Lett. 191*, 39–44.
5. Usher, K. C., Blaszczak, L. C., Weston, G. S., Shoichet, B. K., and Remington, S. J. (1998) Three-dimensional structure of AmpC beta-lactamase from *Escherichia coli* bound to a transition-state analogue: possible implications for the oxyanion hypothesis and for inhibitor design. *Biochemistry 37*, 16082–16092.
6. Guillaume, G., Vanhove, M., Lamotte-Brasseur, J., Ledent, P., Jamin, M., Joris, B., and Frere, J. M. (1997) Site-directed mutagenesis of glutamate 166 in two beta-lactamases. Kinetic and molecular modeling studies. *J. Biol. Chem. 272*, 5438–5444.
7. Lenfant, F., Petit, A., Labia, R., Maveyraud, L., Samama, J. P., and Masson, J. M. (1993) Site-directed mutagenesis of beta-lactamase TEM-1. Investigating the potential role of specific residues on the activity of *Pseudomonas*-specific enzymes. *Eur. J. Biochem. 217*, 939–946.
8. Lobkovsky, E., Moews, P. C., Liu, H., Zhao, H., Frere, J. M., and Knox, J. R. (1993) Evolution of an enzyme activity: crystallographic structure at 2-Å resolution of cephalosporinase from the ampC gene of *Enterobacter cloacae* P99 and comparison with a class A penicillinase. *Proc. Natl. Acad. Sci. U.S.A. 90*, 11257–11261.
9. Minasov, G., Wang, X., and Shoichet, B. K. (2002) An ultrahigh resolution structure of TEM-1 beta-lactamase suggests a role for Glu166 as the general base in acylation. *J. Am. Chem. Soc. 124*, 5333–5340.
10. Bush, K. (1989) Classification of beta-lactamases: groups 2c, 2d, 2e, 3, and 4. *Antimicrob. Agents Chemother. 33*, 271–276.
11. Ledent, P., Raquet, X., Joris, B., Van Beeumen, J., and Frere, J. M. (1993) A comparative study of class-D beta-lactamases. *Biochem. J. 292* (Part 2), 555–562.
12. Ledent, P., and Frere, J. M. (1993) Substrate-induced inactivation of the OXA2 beta-lactamase. *Biochem. J. 295* (Part 3), 871–878.
13. Livermore, D. M. (2002) The impact of carbapenemases on antimicrobial development and therapy. *Curr. Opin. Invest. Drugs 3*, 218–224.
14. Nordmann, P., and Poirel, L. (2002) Emerging carbapenemases in Gram-negative aerobes. *Clin. Microbiol. Infect. 8*, 321–331.
15. Walther-Rasmussen, J., and Hoiby, N. (2006) OXA-type carbapenemases. *J. Antimicrob. Chemother. 57*, 373–383.
16. Queenan, A. M., and Bush, K. (2007) Carbapenemases: the versatile beta-lactamases. *Clin. Microbiol. Rev. 20*, 440–458.
17. Huovinen, P., Huovinen, S., and Jacoby, G. A. (1988) Sequence of PSE-2 beta-lactamase. *Antimicrob. Agents Chemother. 32*, 134–136.
18. Franceschini, N., Boschi, L., Pollini, S., Herman, R., Perilli, M., Galleni, M., Frere, J. M., Amicosante, G., and Rossolini, G. M. (2001) Characterization of OXA-29 from *Legionella* (*Fluoribacter*) *gormanii*: molecular class D beta-lactamase with unusual properties. *Antimicrob. Agents Chemother. 45*, 3509–3516.
19. Girlich, D., Naas, T., and Nordmann, P. (2004) Biochemical characterization of the naturally occurring oxacillinase OXA-50 of *Pseudomonas aeruginosa*. *Antimicrob. Agents Chemother. 48*, 2043–2048.
20. Sun, T., Nukaga, M., Mayama, K., Braswell, E. H., and Knox, J. R. (2003) Comparison of beta-lactamases of classes A and D: 1.5-Å crystallographic structure of the class D OXA-1 oxacillinase. *Protein Sci. 12*, 82–91.
21. Golemi, D., Maveyraud, L., Vakulenko, S., Samama, J. P., and Mobashery, S. (2001) Critical involvement of a carbamylated lysine in catalytic function of class D beta-lactamases. *Proc. Natl. Acad. Sci. U.S.A. 98*, 14280–14285.
22. Danel, F., Frere, J. M., and Livermore, D. M. (2001) Evidence of dimerisation among class D beta-lactamases: kinetics of OXA-14 beta-lactamase. *Biochim. Biophys. Acta 1546*, 132–142.
23. Danel, F., Paetzel, M., Strynadka, N. C., and Page, M. G. (2001) Effect of divalent metal cations on the dimerization of OXA-10 and -14 class D beta-lactamases from *Pseudomonas aeruginosa*. *Biochemistry 40*, 9412–9420.

24. Danel, F., Hall, L. M., Gur, D., and Livermore, D. M. (1995) OXA-14, another extended-spectrum variant of OXA-10 (PSE-2) beta-lactamase from *Pseudomonas aeruginosa*. *Antimicrob. Agents Chemother. 39*, 1881–1884.
25. Pernot, L., Frenois, F., Rybkine, T., L'Hermite, G., Petrella, S., Delettre, J., Jarlier, V., Collatz, E., and Sougakoff, W. (2001) Crystal structures of the class D beta-lactamase OXA-13 in the native form and in complex with meropenem. *J. Mol. Biol. 310*, 859–874.
26. Paetzel, M., Danel, F., de Castro, L., Mosimann, S. C., Page, M. G., and Strynadka, N. C. (2000) Crystal structure of the class D beta-lactamase OXA-10. *Nat. Struct. Biol. 7*, 918–925.
27. Maveyraud, L., Golemi-Kotra, D., Ishiwata, A., Meroueh, O., Mobashery, S., and Samama, J. P. (2002) High-resolution X-ray structure of an acyl-enzyme species for the class D OXA-10 beta-lactamase. *J. Am. Chem. Soc. 124*, 2461–2465.
28. Maveyraud, L., Golemi, D., Kotra, L. P., Tranier, S., Vakulenko, S., Mobashery, S., and Samama, J. P. (2000) Insights into class D beta-lactamases are revealed by the crystal structure of the OXA10 enzyme from *Pseudomonas aeruginosa*. *Structure 8*, 1289–1298.
29. Leonard, D. A., Hujer, A. M., Smith, B. A., Schneider, K. D., Bethel, C. R., Hujer, K. M., and Bonomo, R. A. (2008) The role of OXA-1 beta-lactamase Asp(66) in the stabilization of the active-site carbamate group and in substrate turnover. *Biochem. J. 410*, 455–462.
30. Dementin, S., Bouhss, A., Auger, G., Parquet, C., Mengin-Lecreulx, D., Dideberg, O., van Heijenoort, J., and Blanot, D. (2001) Evidence of a functional requirement for a carbamoylated lysine residue in MurD, MurE and MurF synthetases as established by chemical rescue experiments. *Eur. J. Biochem. 268*, 5800–5807.
31. Shibata, N., Yamamoto, H., Inoue, T., Uemura, K., Yokota, A., and Kai, Y. (1996) Crystallization and preliminary crystallographic studies of ribulose 1,5-bisphosphate carboxylase/oxygenase from a red alga, *Galdieria partita*, with a high specificity factor. *J. Biochem. 120*, 1064–1066.
32. Kimlova, L. J., Pyne, C., Keshavjee, K., Huy, J., Beebakhee, G., and Bognar, A. L. (1991) Mutagenesis of the folC gene encoding folylpolyglutamate synthetase-dihydrofolate synthetase in *Escherichia coli*. *Arch. Biochem. Biophys. 284*, 9–16.
33. De Vos, D., Hulpiau, P., Vergauwen, B., Savvides, S. N., and Van Beeumen, J. (2005) Expression, purification, crystallization and preliminary X-ray crystallographic studies of a cold-adapted aspartate carbamoyltransferase from *Moritella profunda*. *Acta Crystallogr., Sect. F: Struct. Biol. Cryst. Commun. 61*, 279–281.
34. Jabri, E., Carr, M. B., Hausinger, R. P., and Karplus, P. A. (1995) The crystal structure of urease from *Klebsiella aerogenes*. *Science 268*, 998–1004.
35. Morollo, A. A., Petsko, G. A., and Ringe, D. (1999) Structure of a Michaelis complex analogue: propionate binds in the substrate carboxylate site of alanine racemase. *Biochemistry 38*, 3293–3301.
36. Danel, F., Hall, L. M., Gur, D., and Livermore, D. M. (1998) OXA-16, a further extended-spectrum variant of OXA-10 beta-lactamase, from two *Pseudomonas aeruginosa* isolates. *Antimicrob. Agents Chemother. 42*, 3117–3122.
37. Levesque, R. C., and Jacoby, G. A. (1988) Molecular structure and interrelationships of multiresistance beta-lactamase transposons. *Plasmid 19*, 21–29.
38. Hopwood, D. A., and Ferguson, H. M. (1970) Genetic recombination in a thermophilic actinomycete, *Thermoactinomyces vulgaris*. *J. Gen. Microbiol. 63*, 133–136.
39. De Meester, F., Joris, B., Lenzini, M. V., Dehottay, P., Erpicium, T., Dusart, J., Klein, D., Ghuysen, J. M., Frere, J. M., and Van Beeumen, J. (1987) The active sites of the beta-lactamases of *Streptomyces cacaoi* and *Streptomyces albus* G. *Biochem. J. 244*, 427–432.
40. Kabsch, W. (1993) Automatic processing of rotation diffraction data from crystals of initially unknown symmetry and cell constants. *J. Appl. Crystallogr. 26*, 795–800.
41. CCP4 (1994) The CCP4 suite: programs for protein crystallography. *Acta Crystallogr., Sect. D: Biol. Crystallogr. D50*, 760–763.
42. Navaza, J. (2001) Implementation of molecular replacement in AMoRe. *Acta Crystallogr., Sect. D: Biol. Crystallogr. 57*, 1367–1372.
43. Murshudov, G. N., Vagin, A. A., and Dodson, E. J. (1997) Refinement of macromolecular structures by the maximum-likelihood method. *Acta Crystallogr., Sect. D: Biol. Crystallogr. 53*, 240–255.
44. Emsley, P. C., K. (2004) Coot: model-building tools for molecular graphics. *Acta Crystallogr., Sect. D: Biol. Crystallogr. 60*, 2126–2132.
45. DeLano, W. L. (2002) The PyMOL Molecular Graphics System, DeLano Scientific, San Carlos, CA.
46. Kraus, L. M., Gaber, L., Handorf, C. R., Marti, H. P., and Kraus, A. P., Jr. (2001) Carbamoylation of glomerular and tubular proteins in patients with kidney failure: a potential mechanism of ongoing renal damage. *Swiss Med. Wkly. 131*, 139–134.
47. Kraus, L. M., Miyamura, S., Pecha, B. R., and Kraus, A. P., Jr. (1991) Carbamoylation of hemoglobin in uremic patients determined by antibody specific for homocitrulline (carbamoylated epsilon-N-lysine). *Mol. Immunol. 28*, 459–463.
48. Pratt, R. F., Dryjanski, M., Wun, E. S., and Marathias, V. M. (1996) 8-Hydroxypenillic acid from 6-aminopenicillanic acid: a new reaction catalyzed by a class C Î²-lactamase. *J. Am. Chem. Soc. 118*, 8207–8212.
49. Poirel, L., Girlich, D., Naas, T., and Nordmann, P. (2001) OXA-28, an extended-spectrum variant of OXA-10 beta-lactamase from *Pseudomonas aeruginosa* and its plasmid- and integron-located gene. *Antimicrob. Agents Chemother. 45*, 447–453.
50. Schneider, K. D., Bethel, C. R., Distler, A. M., Hujer, A. M., Bonomo, R. A., and Leonard, D. A. (2009) Mutation of the active site carboxy-lysine (K70) of OXA-1 beta-lactamase results in a deacylation-deficient enzyme. *Biochemistry 48*, 6136–6145.